

Application of Remote Sensing and GIS for Evaluation of Coastal Protection Methods and Shoreline Change: A Case Study of Bardaweil Lagoon, Sinai Peninsula, Egypt [†]

Kamal Darwish *

Department of Geography, Faculty of Arts, Minia University, El Minia 61519, Egypt

* Correspondence: kamal.srogy@mu.edu.eg; Tel.: +2-01093566658

[†] Presented at the 6th International Electronic Conference on Water Sciences (ECWS-6), Online, 15–30 November 2021.

Abstract: This study aims to evaluate the effectiveness of the coastal protection engineering methods along western Bardaweil Lagoon artificial Inlets. A Multi-temporal shorelines were detected and extracted from Landsat satellite time-series images (30-m spatial resolution) including different sensors ; Thematic Mapper (TM), Enhanced Thematic Mapper (ETM+), and Operational Land Imager(OLI) imagery taken from 1985 to 2020 were used to compare shoreline change rates prior to and after the construction of the coastal structures (Jetties). Geographic Information Systems based Digital Shoreline Analysis System (DSAS) has been used to compute statistics of historical shoreline changes. The results indicated that the coastal structures were successful to protect the navigational canals of Inlets from sedimentation, as well as it contributes to save lagoon inlets from severe coastal erosion, on the other hand, a new coastal erosion zones have been appeared close to the inlets entrance and need to protection.

Keywords: coastline dynamics; coastal lagoons; North Sinai Coast; coastal protection methods; DSAS; GIS analysis

Citation: Darwish, K. Application of Remote Sensing and GIS for Evaluation of Coastal Protection Methods and Shoreline Change: A Case Study of Bardaweil Lagoon, Sinai Peninsula, Egypt. *Environ. Sci. Proc.* **2021**.

Academic editor: Marcel J.F. Stive

Publisher's Note: MDPI stays neutral with regard to jurisdictional claims in published maps and institutional affiliations.



Copyright: © 2021 by the authors. Submitted for possible open access publication under the terms and conditions of the Creative Commons Attribution (CC BY) license (<https://creativecommons.org/licenses/by/4.0/>).

1. Introduction

Coastline is the boundary between land and the sea, it considers one of the 27 most important land surface features, and it is vulnerable to natural processes such as coastal erosion/accretion, sea level changes and human activities [1]. Studies of changing shorelines is important to evaluate coastal protection [2,3], apply numerical models [4,5], developing hazard maps [6], draw policies regarding coastal development [7], and for coastal management and monitoring [8].

Coastline changes are usually studied using ground surveying and aerial photogrammetry techniques [9,10]. Although, availability and affordability of remote sensing recently, it has become a suitable technique for monitoring coastal dynamics in a fast and cost effective way. Remote sensing images of medium spatial resolution (30-m spatial resolution) have been used globally for coastline change monitoring and analysis since the public availability of the United States Geological Survey (USGS) in 2008. The availability and frequency of Landsat time-series images from different sensors, including Multispectral Scanner (MSS), Thematic Mapper (TM), Enhanced Thematic Mapper Plus (ETM+) and latest Operational Land Imager (OLI), are suitable for monitoring coastline changes in large areas and it is enable effective extraction of coastlines [11].

The spectral water indices based on water body mapping methods are widely used for coastline extraction from Landsat images because of their reliability, user friendliness and low computation cost [12]. In the past decades, different water indices developed for water body mapping. It was started by McFeeter [13] proposed the normalized difference

water index (NDWI) using a ratio of the green and the near infrared (NIR) bands to enhance the presence of water features in remotely sensed imagery. Xu [14] developed a new index, namely as modified normalized difference water index (MNDWI), by improving the NDWI with the substitution of the middle-infrared (MIR) band, such as Landsat TM band 5, for the NIR bands.

Previous studies were assessed the shoreline morphodynamics in study area using remote sensing started by El Banna and Hereher [15], which assessed the shoreline change along North Sinai coast using Landsat images from 1986 to 2001. Nassar et al. [16,17] assessed shoreline changes along the North Sinai coast using geographic information system and digital shoreline analysis system (DSAS) during the elapsed period from 1989 to 2016. The measurement of shoreline variation is mainly described for three zones: zone I, El-Tinah plain bay; zone II, El-Bardawil Lake; zone III, El-Arish valley. Nassar et al. [18] studied the Numerical simulation of shoreline responses near the western artificial inlet of the Bardawil Lagoon. In addition, there are regional studies evaluated the effectiveness of Coastal Protection Methods Using Remote Sensing and GIS-based DSAS techniques have introduced by Darwish et al. [19] along Nile Delta Coast, Elkafrawy et al. [20] along Brullus Headland.

In this study, a geospatial techniques using geographic information systems (GIS) and automatic computation (DSAS), of the coastline changes of Bardaweil Lagoon Artificial Inlets (1985–2020) were detected and extracted based on Landsat time-series images using the spectral water indices (NDWI and MNDWI). Several statistical approach have been used for determining the rates of shoreline changes, including End Point Rates (EPR), Linear Regression Rates (LRR) and Net Shoreline Movement (NSM). The main objective of this work is to map and quantify the erosion and accretion areas and to evaluate the long-term rates of shoreline changes along the western artificial inlets of Bardaweil lagoon.

2. Materials and Methods

2.1. Study Area

Bardaweil Lagoon is located on along the Mediterranean coast of Egypt (Figure 1). It extends from the east of El-Tinah Plain to the west of the El Arish thermal power plant. It is connected to the Mediterranean Sea by three inlets, two Jetties have been constructed to the east and west of inlets (1) and (2) since 1991 to maintain and protect the inlets from the accumulation of coastal sediments and coastal erosion. The lengths of these jetties for inlets (1) and (2) are approximately 300 m and 700 m, respectively. These jetties have fundamentally helped to maintain these inlets, but their presence has led to an undesirable evolution of the shoreline by causing coastal erosion and extreme forwarding of the coastline offshore [18]. The climate setting of the study area is an arid; the average maximum temperature is 32.5° C in summer and a minimum of 10° C in winter. Rainfall increases towards the east and rapidly decreases towards the south. It varies from a low of approximately 75 mm/year at Port Said, to more than 130 mm/year at El Arish and about 244 mm/year at Rafah. The wind speed recorded monthly at the meteorological stations in El Arish, Port Said, and Ismailia ranges from 2.6 to 11.3 m/s. The northern part of Sinai is subject to sandstorms, called El-Khamasin, which blow from the south and the southwest intermittently over a period of 50 days during February and March [15]. The marine climate of wave action along the Mediterranean coast of Egypt is seasonal in intensity and direction. Low (swell) waves prevail during spring and summer, with wave heights (1.16 m) and the prevailing wave direction is NW. Winter waves can be much higher, fluctuating between storm and calm and coming from the N, NNW and NW. The overall maximum wave height is (4.25 m) [17].

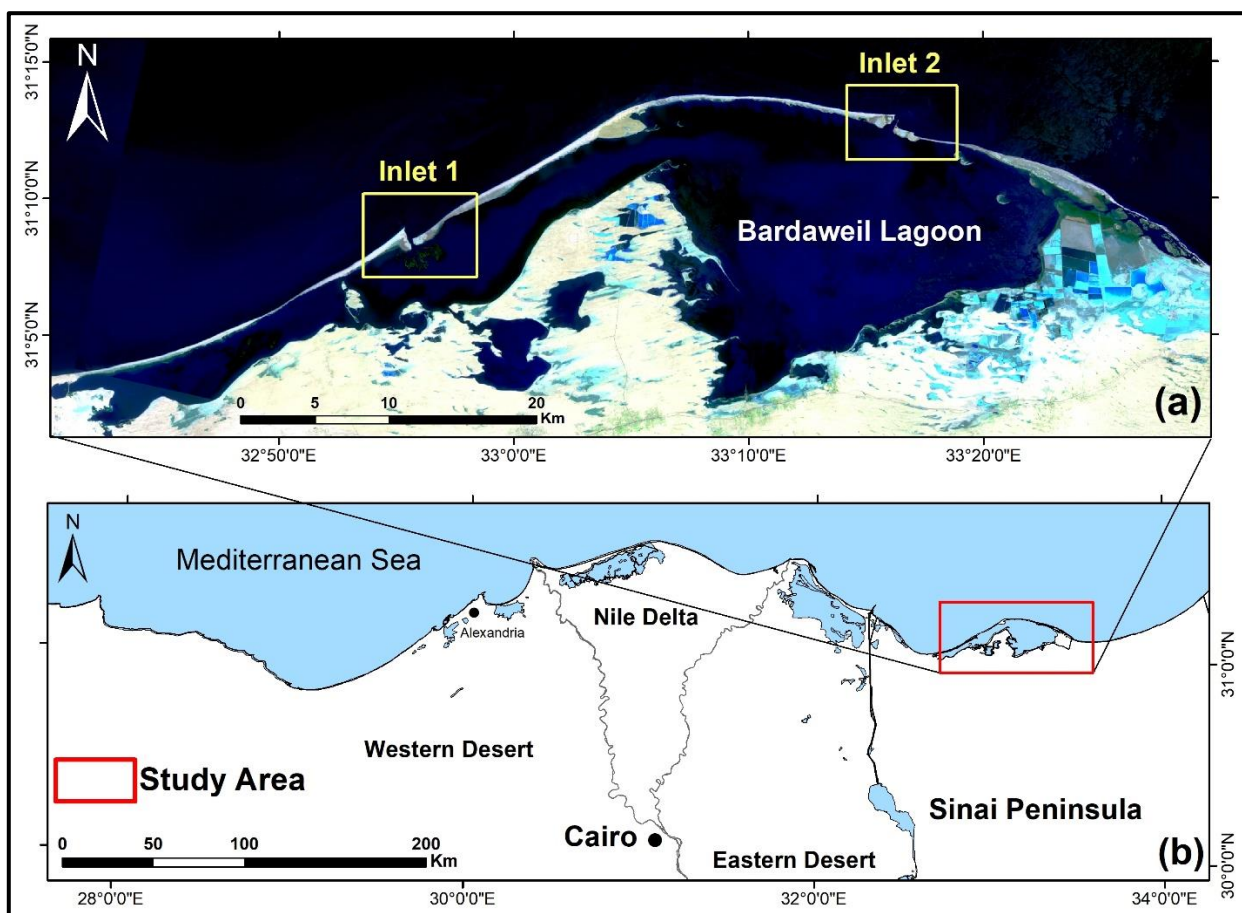


Figure 1. Location Map of the study area. Sub-figure (a) shows the artificial Inlets of Bardaweil Lagoon from Landsat-8 imagery 2020, and Sub-figure (b) shows the location of the study area within Northern Egypt.

2.2. Materials

Landsat series images from 1985 to 2020 covering a time span of 35 years were used as data sources to analyse the Bardaweil Lagoon Inlets. The images have been acquired in summer season and in good quality, with no effective clouds. The satellite remote sensing images as shown in Table 1, including Landsat-5 Thematic Mapper (TM), Landsat-7 Enhanced Thematic Mapper Plus, Landsat-8 Operational Land Imager (OLI). All the Landsat series images were downloaded in the GeoTIFF format from the United States Geological Survey (USGS) Earth Explorer Website (<http://earthexplorer.usgs.gov/>). These Landsat datasets constitute the useable database of good quality (level 2 product), radiometrically corrected to Surface Reflectance, free of clouds (at least covering the coastlines of interest) and sensor defects, such as striping or banding.

Table 1. Details of Landsat-time series satellite images used in this study.

Acquired Date	Satellite/Sensor	Level ¹	Path/Row	Pixel Size (m)
06.12.1985	Landsat-5/TM	L2SP	175/38	30
05.25.1990	Landsat-5/TM	L2SP	175/38	30
07.31.2000	Landsat-7/ETM+	L2SP	175/38	30
06.17.2010	Landsat-5/TM	L2SP	175/38	30
06.12.2020	Landsat-8/OLI/TIRS	L2SP	175/38	30

¹ Surface Reflectance Radiometric Calibration, all Landsat images freely downloaded from USGS Website: <https://earthexplorer.usgs.gov/>.

2.3. Methods

To achieve the goals of this study, three steps are followed; (1) remotely sensed data collection and preprocessing such as band combination, geometrical and radiometric corrections. (2) Shoreline extraction prior to and after construction of Jetties using NDWI/MNDWI indices and accuracy of the extracted shorelines were assessed using Google Earth data. (3) GIS based spatial analysis of shoreline changes using Digital Shoreline Analysis System (DSAS) is a GIS-based system established by the USGS. DSAS calculates gaps amongst the coastline positions during defined periods (Figure 2). Normalized Difference Water Index (NDWI)/Modified Normalized Difference Water Index (MNDWI) water indices applied for study area using ERDAS Imagine 2015 algorithms to detect the water/land feature by thresholding method using ENVI 5.3 software for coastline detection as shown in Figure (2). NDWI was proposed by McFeeters (1996) for water resource assessment. An NIR band and a green band are used to enhance the discrepancies between surface water and non-water features [21]. McFeeters’s NDWI is calculated in equation (1) as:

$$NDWI = \frac{(Band_{Green} - Band_{NIR})}{(Band_{Green} + Band_{NIR})} \tag{1}$$

where $Band_{Green}$ is the reflectance value of the green band and $Band_{NIR}$ reflection value of the NIR band. The derived new index is called MNDWI [22], which is expressed in equation (2) as:

$$MNDWI = \frac{Band_{Green} - Band_{MIR}}{Band_{Green} + Band_{MIR}} \tag{2}$$

where $Band_{MIR}$ is the reflectance of the MIR band.

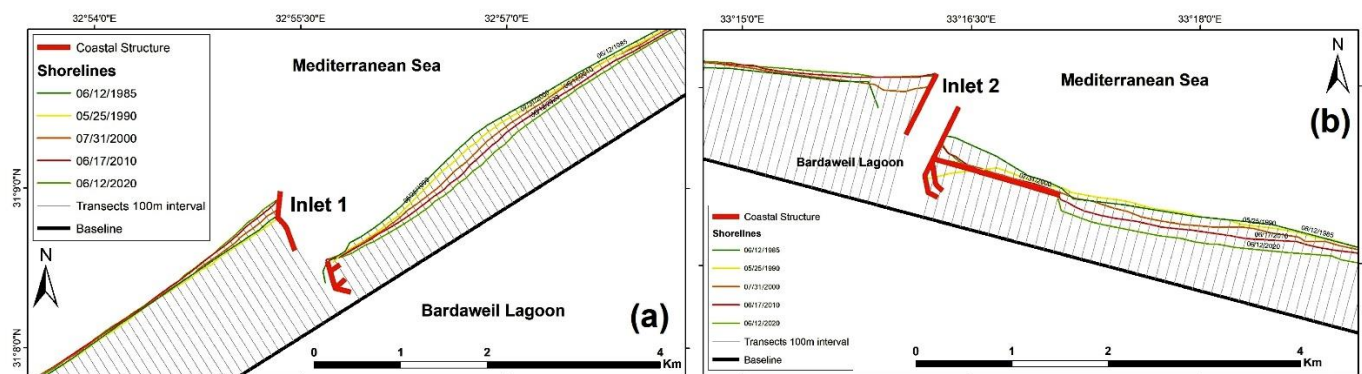


Figure 2. DSAS- based Shoreline changes Analysis along western Bardaweil Artificial Inlets from 1985 to 2020. Sub-figure (a) shows Inlet-1, and Sub-figure (b) shows Inlet-2.

3. Results

The results of shoreline change analysis along two artificial inlets of Bardaweil lagoon indicated show a similarity of shoreline change pattern, trends, and effects of coastal protection works as shown from Table 2 and Figure 3.

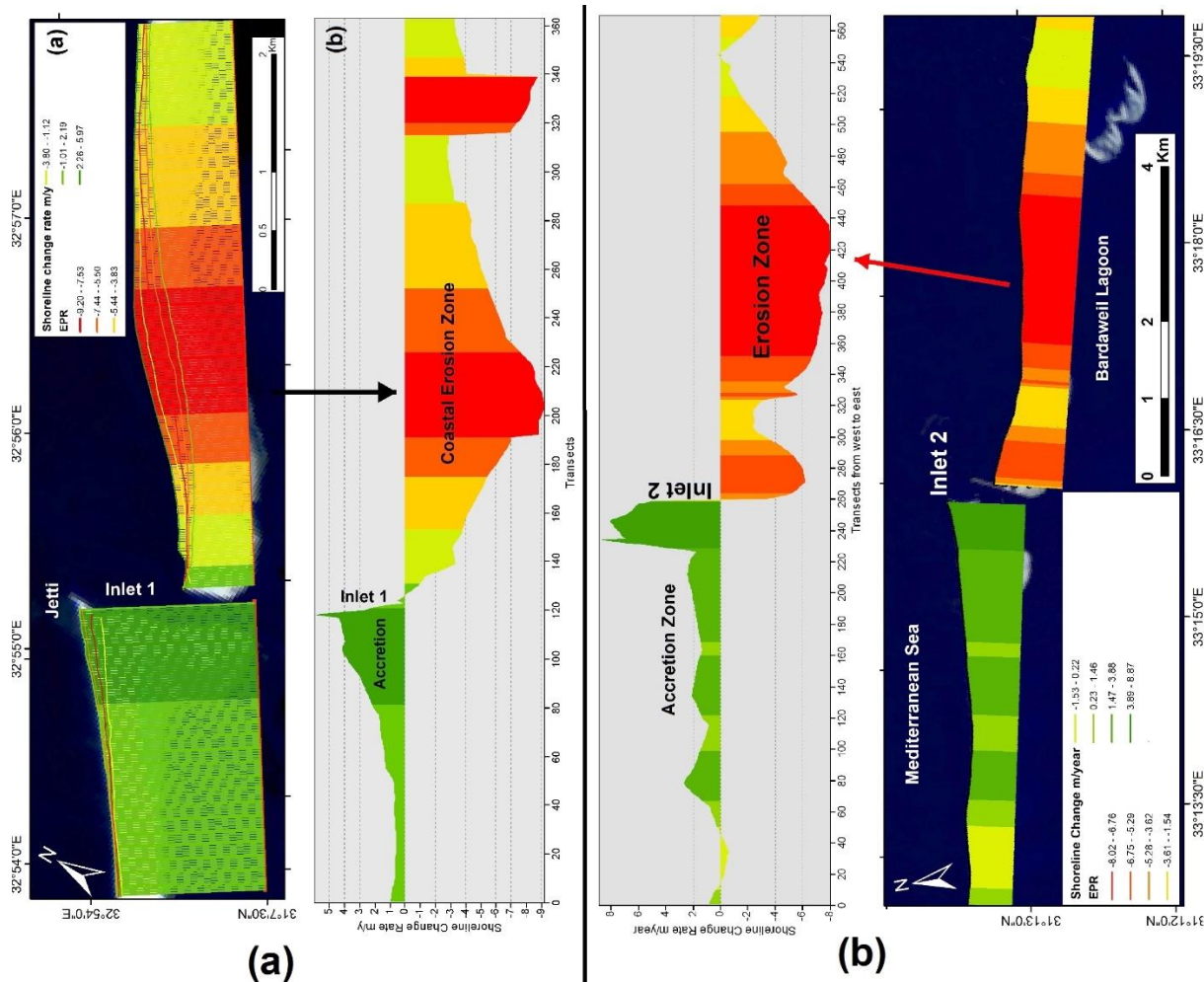
Inlet-1:

The analysis shows that two zones of coastal changes behind and in front of the Jetty, Its appear that shoreline advanced behind the Jetty with a distance 179.4 m with a maximum annual rate +5.7 m/y and an average is 1.8 m/y. While, zone2 located ahead toward the east, in this zone the total retreat distance is -183.2 m with a maximum annual rate -9.2 m/y and an average -5.2 m/y.

Inlet-2:

The analysis of 11 km coastline sector covering the second artificial Inlet-2 from 1985 to 2020, shows that a two coastal zones. The first accretion zone appears behind the Jetty toward the west with total advance distance 310 m, the maximum annual rate is +8.9m /y and average is +1.9m/y. The second zone shows an erosion area with total retreat distance is -280.6 m and a maximum annual rate is -8.2 m/y and an average (-4.8 m/y).

145
146
147
148
149



150
151
152

Figure 3. Shoreline Change Detection along Bardaweil Lagoon Inlets between 1985 and 2020. Subfigure (a) shows shoreline changes along Inlet-1, and subfigure (b) shows shoreline change rates along Inlet-2.

Table 2. Statistics of Shoreline Changes between 1985 and 2020.

153

	Inlet-1		Inlet-2	
	Zone I	Zone II	Zone I	Zone II
No. of Transects	120	240	260	311
Length (km)	2.4	4.8	5.2	6.2
NSM (m)	H	+179.4	-321.9	+310.5
	M	+62.2	-183.3	+59.2
EPR (m/year)	H	+5.97	-9.2	8.9
	M	+1.8	-5.2	+1.9
LRR (m/year)	H	+6.3	-8.9	+9.4
	M	+2.23	-4.9	+2.0

NSM= Net Shoreline Movement, EPR= End Point Rate, LRR= Linear Regression Rate. H= Highest Rate, M= Mean Rate. (+) refer to accretion, (-) refer to Erosion.

154
155

Table 3, and Figure 4, shows a shoreline change rates prior to and after the construction of coastal protection devises along the Bardaweil lagoon Inlets. The analysis indicated that Jetties were successful to protect the inlets from erosion and sedimentation in the navigational channels, It was reserved the deposits from the littoral currents formed an accretion zone behind the Jetty (+9.33m/y and +35.2 m/y) for Inlet-1, and Inlet-2 respectively. On the other hand, anew coastal erosion zone has been appeared toward the east (-10.3, and -11.83 m/y) along Inlet-1 zone2, and Inlet-2 zone2, respectively.

Table 3. Evaluation of Coastal Protection Methods along two artificial Inlets.

		Inlet-1				Inlet-2			
		Before		After		Before		After	
		Zone I	Zone II	Zone I	Zone II	Zone I	Zone II	Zone I	Zone II
Length (km)		2.4	4.8	2.4	4.8	5.2	6.2	5.2	6.2
EPR (m/y)	H	-6.7	-17.6	+9.33	-10.3	-12.91	-62.96	+35.2	-11.83
	M	-3.0	-10.0	+3.55	-3.7	-0.37	-1.67	+4.04	-4.04

Before = (1985-1990), After = (1990-2000). H= Highest Shreline Rate, M= Mean Shoreline Change Rate.

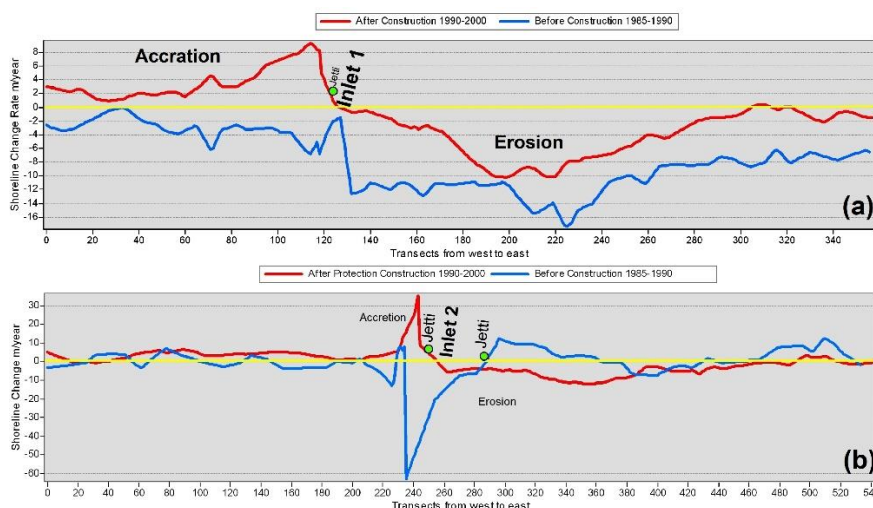


Figure 4. Shoreline change rates before (1985-1990) and after (1990-2000) coastal protection construction along Bardaweil Lagoon Inlets. Subfigure (a) shows Inlet-1, and subfigure (b) shows Inlet-2.

4. Discussion

The Long-term analysis of shoreline around Bardaweil lagoon artificial inlets reveals coastal accretion zone behind the Jetty and coastal erosion zone unprotected formed along shore eastward on both inlets, as well as the evaluation of the effectiveness of coastal structure indicated that Jetties have been reversed the shoreline erosion rates prior to construction of jetties to accretion after the construction. The negative impacts of Jetties are new severe coastal erosion zone has been formed and rates increased gradually because of the reduction of upcoming sediments feeding the coast which reserved behind the Jetties.

5. Conclusions

Assessment of shoreline changes using multi-temporal remote sensing data and GIS techniques is very effective techniques for coastal management, Planning and coastal engineering protection methods evaluation by measuring the spatial distribution of shoreline change prior to and after the coastal protection devises construction. In this study, remote sensing and GIS integration help to mapping coastal erosion and accretion zones. The coastal protection methods stopped the flow of suspended sediments toward the east, and caused a new-severe coastal erosion zones need to protection with short groins, and

breakwaters. It is recommended to establish a new-coastal protection works to conserve the coast from the severe erosion. 185
186

Funding: This research received no external funding. 187

Institutional Review Board Statement: Not applicable. 188

Informed Consent Statement: Informed consent was obtained from all subjects involved in the study. 189
190

Data Availability Statement: Not applicable. 191

Conflicts of Interest: The authors declare no conflict of interest. 192

References 193

1. Liu, Y.; Wang, X.; Ling, F.; Xu, S.; Wang, C. Analysis of Coastline Extraction from Landsat-8 OLI Imagery. *Water* **2017**, *9*, 816. 194
2. Zanuttigh, B.; Martinelli, L.; Lamberti, A.; Moschella, P.; Hawkins, S.; Marzetti, S.; Ceccherelli, V.U. Environmental design of coastal defence in Lido di Dante, Italy. *Coast. Eng.* **2005**, *52*, 1089–1125. 195
196
3. Jin, D.; Hoagland, P.; Au, D.K.; Qiu, J. Shoreline change, seawalls, and coastal property values. *Ocean Coast. Manag.* **2015**, *114*, 185–193. 197
198
4. Baldassarre, G.D.; Schumann, G.; Bates, P.D. A technique for the calibration of hydraulic models using uncertain satellite observations of flood extent. *J. Hydrol.* **2009**, *367*, 276–282. 199
200
5. Kaergaard, K.; Fredsoe, J. A numerical shoreline model for shorelines with large curvature. *Coast. Eng.* **2013**, *74*, 19–32. 201
6. Snoussi, M.; Ouchani, T.; Khouakhi, A.; Niang-Diop, I. Impacts of sea-level rise on the Moroccan coastal zone: Quantifying coastal erosion and flooding in the Tangier Bay. *Geomorphology* **2009**, *107*, 32–40. 202
203
7. O'Connor, M.C.; Cooper, J.A.G.; McKenna, J.; Jackson, D.W.T. Shoreline management in a policy vacuum: A local authority perspective. *Ocean Coast. Manag.* **2010**, *53*, 769–778. 204
205
8. Tamassoki, E.; Amiri, H.; Soleymani, Z. Monitoring of shoreline changes using remote sensing (case study: Coastal city of Bandar Abbas). In 7th IGRSM International Remote Sensing & GIS Conference and Exhibition; IOP Publishing: Bristol, UK, 2014; Volume 20. 206
207
208
9. Dewi, R.S.; Bijker, W.; Stein, A.; Marfai, M.A. Fuzzy classification for shoreline change monitoring in a part of the northern coastal area of Java, Indonesia. *Remote Sens.* **2016**, *8*, 190. 209
210
10. Ghosh, M.K.; Kumar, L.; Roy, C. Monitoring the coastline change of Hatiya Island in Bangladesh using remote sensing techniques. *ISPRS J. Photogramm. Remote Sens.* **2015**, *101*, 137–144. 211
212
11. Du, Z.; Li, W.; Zhou, D.; Tian, L.; Ling, F.; Wang, H.; Gui, Y.; Sun, B. Analysis of Landsat-8 OLI imagery for land surface water mapping. *Remote Sens. Lett.* **2014**, *5*, 672–681. 213
214
12. Cui, B.; Li, X. Coastline change of the Yellow River estuary and its response to the sediment and runoff (1976–2005). *Geomorphology* **2011**, *127*, 32–40. 215
216
13. McFeeters, S.K. The use of the Normalized Difference Water Index (NDWI) in the delineation of open water features. *Int. J. Remote Sens.* **1996**, *17*, 1425–1432. 217
218
14. Xu, H. Modification of normalized difference water index (NDWI) to enhance open water features in remotely sensed imagery. *Int. J. Remote Sens.* **2006**, *27*, 3025–3033. 219
220
15. El Banna, M.; Hereher, M. Detecting temporal shoreline changes and erosion/accretion rates, using remote sensing, and their associated sediment characteristics along the coast of North Sinai, Egypt. *Environ. Geol.* **2009**, *58*, 1419–1427. 221
222
16. Nassar, K.; Mahmod, W.E.; Fath, H.; Masria, A.; Nadaoka, K.; Negm, A. Shoreline change detection using DSAS technique: Case of North Sinai coast, Egypt. *Mar. Georesources Geotechnol.* **2019**, *37*, 1, 81–95. 223
224
17. Nassar, K.; Fath, H.; Mahmod, W.E. Automatic detection of shoreline change: Case of North Sinai coast, Egypt. *J. Coast Conserv.* **2018**, *22*, 1057–1083. <https://doi.org/10.1007/s11852-018-0613-1>. 225
226
18. Nassar, K.; Mahmod, W.E.; Masria, A.; Fath, H.; Nadaoka, K. Numerical simulation of shoreline responses in the vicinity of the western artificial inlet of the Bardawil Lagoon, Sinai Peninsula, Egypt. *Appl. Ocean Res.* **2018**, *74*, 87–101, ISSN 0141-1187. <https://doi.org/10.1016/j.apor.2018.02.015>. 227
228
229
19. Darwish, K.; Smith, S.E.; Torab, M.; Monsef, H., and Hussein, O. Geomorphological changes along the Nile Delta coastline between 1945 and 2015 detected using satellite remote sensing and GIS. *J. Coast. Res.* **2017**, *33*, 786–794. 230
231
20. Elkafrawy, S.B.; Basheer, M.; Mohamed, H.; Naguib, D.M. Applications of remote sensing and GIS techniques to evaluate the effectiveness of coastal structures along Burullus headland-Eastern Nile Delta, Egypt. *Egypt. J. Remote. Sens. Space Sci.* **2021**, *24*, 247–254. 232
233
234
21. McFeeters, S.K. The use of the Normalized Difference Water Index (NDWI) in the delineation of open water features. *Int. J. Remote Sens.* **1996**, *17*, 1425. 235
236
22. Xu, H. Modification of normalized difference water index (NDWI) to enhance open water features in remotely sensed imagery. *Int. J. Remote Sens.* **2006**, *27*, 3025–3033. 237
238